sciendo

Polish Journal of Chemical Technology, 23, 2, 60—65, 10.2478/pjct-2021-0018

Time-dependent growth of the dendritic silver prepared using square wave voltammetry technique for methylene blue photodegradation

Setia Budi*, Lintang Dhanasmoro, Agung Purwanto, Sukro Muhab

Department of Chemistry, Faculty of Mathematics and Natural Sciences, Universitas Negeri Jakarta, Jl. Rawamangun Muka, Jakarta 13220, Indonesia
**Corresponding author: e-mail: setiabudi@unj.ac.id*

Silver (Ag) particle is a promising photocatalyst material with relatively high catalytic activity and good absorption in the visible light region. A dendritic structure of Ag has been studied in the purpose to enhance photocatalytic activity due to a large surface area and active site number of the metallic Ag particles. In this work, the Ag dendritic structure was synthesized from a surfactant-free electrolyte using the square wave voltammetry technique. The time-dependent growth of the Ag dendrites and their photocatalytic activity on methylene blue (MB) photodegradation are reported. Morphological analysis exhibits the fractal dendritic structure of Ag was found to continuously grow by increasing the deposition time. The Ag dendrites showed a low charge transfer resistance (366.21 Ω) and high specific capacitance (2.09 F/g). A high rate of MB degradation (45.57%) under ultraviolet irradiation indicated that the Ag dendrites produced using this technique are effective for the photocatalytic degradation of MB dye.

Keywords: Square-wave voltammetry, dendritic Ag, photocatalysis, photodegradation of methylene blue.

INTRODUCTION

Photocatalysis is considered a promising method for degrading organic pollutants and has been widely studied due to its low cost, environmental friendliness, and low risk of generating new toxicants[1, 2]. Among photocatalyst materials, silver nanoparticles have been considered as potential metallic-based photocatalyst due to good absorption capability in the visible light region[3, 4]. In addition, silver is stable, exhibits superior electrocatalytic activity, and has good reproducibility and optical cross-sectional characteristics[5–7].

Modifying morphology of the nanostructures is a potential approach to obtain high levels of catalytic activity. Numerous synthetic routes have been developed to produce various Ag photocatalyst shapes, including wires[8], rods[9], sheets [10] and dendrites. Ag dendrites with multilevel branching structures stand out among other nanostructures due to their large specific surface area that provides large active sites at the ends of their branches or between adjacent Ag branches[13]. Among preparation methods, electrodeposition has been utilized to prepare different shapes of metallic nanoparticles[14]. To produce a dendritic structure of Ag, various electrodeposition techniques such as potentiostatic[15, 16] and galvanostatic[17, 18] have been reported. The use of surfactants[19–21] and templates[17, 22] were also investigated to obtain the desired structures. However, preparation of the dendritic structure in an additive-free solution remains challenging.

Square wave voltammetry is another technique that has been reported to be successfully employed for platinum (Pt) nanodendrite preparation. In this technique, a large-amplitude interval as a symmetrical square wave is employed to the working electrode. Moreover, the shape of fine Pt dendrites could be controlled by adjusting the pulse potentials[23]. This report describes the advantage of the square wave voltammetry technique for developing the multilevel structure of the metallic particle. In this work, the square wave voltammetry technique was employed in the preparation of Ag dendrite structure from a surfactant-free electrolyte. The growth of the Ag structure was observed at different deposition times. The as-prepared dendrites were then examined to investigate their electrochemical properties and photocatalytic activity. The photocatalytic activity toward methylene blue, which is known for its poor degradation and the cause of health problems, was also studied[24, 25].

MATERIALS AND METHODS

Materials

Silver nitrate ($AgNO_3$) and nitric acid (HNO_3) were supplied by PT. Merck Indonesia. The chemicals were analytical grade reagents and used for electrolytes preparation without further purification. Indium tin oxide (ITO) coated polyethylene terephthalate (PET) was purchased from Kintec Company. The substrate was rinsed with ethanol and double-distilled water before electrodeposition.

Synthesis of Ag dendrites

The Ag dendrites were prepared from the electrolytes containing 0.5 mM $AgNO_3$ and 0.1 mM HNO_3. The electrodeposition was carried out by square wave voltammetry techniques using an EA 163 eDAQ potentiostat in a three-electrode electrochemical cell. A platinum plate with 1 x 1 cm^2 size and Ag/AgCl were used as the counter and reference electrodes, respectively. Indium tin oxide-coated polyethylene terephthalate (ITO-PET) was used as a substrate for the deposition of Ag. The electrodeposition was conducted at room temperature with upper and lower potentials of 1.75 V (Ag/AgCl) and –0.3 V (Ag/AgCl), respectively. The potential pulse duration was 100 ms, and the deposition times were varied from 1 to 20 minutes.

Characterization

The as-prepared Ag dendrites were analyzed under a scanning electron microscope (FESEM, FEI Quanta 650). The presence of Ag was verified through an energy dispersive X-ray (EDX) spectrometer coupled to the FESEM. The electrochemical properties were examined using cyclic voltammetry (CV) and electrochemical impedance spectroscopy (EIS) techniques. The cyclic voltammetry measurement was carried out using

an EA163 eDAQ potentiostat within the voltage range of −0.9 V to −0.2 V. Furthermore, EIS measurements were conducted by an ERZ100 eDAQ electrochemical impedance analyzer within a frequency range of 1 Hz to 10 kHz. Both CV and EIS measurements were conducted in an electrolyte containing 0.5 M KCl. All measurements were carried out at room temperature.

Photodegradation Assays of Methylene Blue

The photocatalytic properties of the Ag dendrites were studied by examining the photodegradation of MB under ultraviolet (UV) radiation. This photodegradation performance was evaluated by recording the absorption spectrum of MB for 30 min using a GBC Cintra 2020 spectrophotometer.

RESULTS AND DISCUSSION

Morphological and structural characterization

Figure 1 shows SEM micrographs which indicate the evolution of the morphology of Ag dendrites at different deposition times. Figure 1a exhibits the presence of Ag particles on the substrate, which represents the initial growth stage at a deposition time of 1 minute. Ag dendrites with main trunks and secondary branches were found to be formed at the deposition time of 5 min (Fig. 1b). When deposition time increased, the dendrites extended considerably and grew larger with more pronounced high-order branches assembled a dendritic fractal structure (Fig. 1c–d). The formation of fractal structures of Ag dendrites could be associated with the two different applied potentials during sample preparation that controlled using the square wave voltammetry technique. At upper potential (E_u), 1.7 V vs Ag/AgCl, the electric field drove the Ag ions to move toward the working electrode and then adsorbed on the surface. The adsorbed ions were reduced to Ag metals that initiated to form a nucleus of the Ag particle on the active site lied over the ITO surface. The nucleus then grew along the pulse period. When the applied voltage switched to the lower potential (E_l), –300 mV vs Ag/AgCl, the particles growth ceased due to nonequilibrium conditions as a consequence of more negative voltage than those of Ag reduction potential. A previous study reported that at low potential, the reduced metal atoms on the high surface energy region tend to diffuse to low surface energy area and produced a thermodynamically stable morphology shape[23]. Subsequent nucleus formation that followed by particle growth of Ag recurred when the potential was returned to the upper value. The new nucleus was formed on the previously deposited Ag particles rather than on the bare substrate as a consequence of a low activation overpotential desired for the Ag ions reduction[26, 27]. Hence, this mechanism facilitated the continuous nucleation and particle growth resulted in the fractal structure of dendritic Ag through the oriented attachment process. Figure 2 exhibits the EDX spectrum that revealed the presence of the Ag in the deposit obtained through a square wave voltammetry deposition, while the rest of the elements came from the substrate.

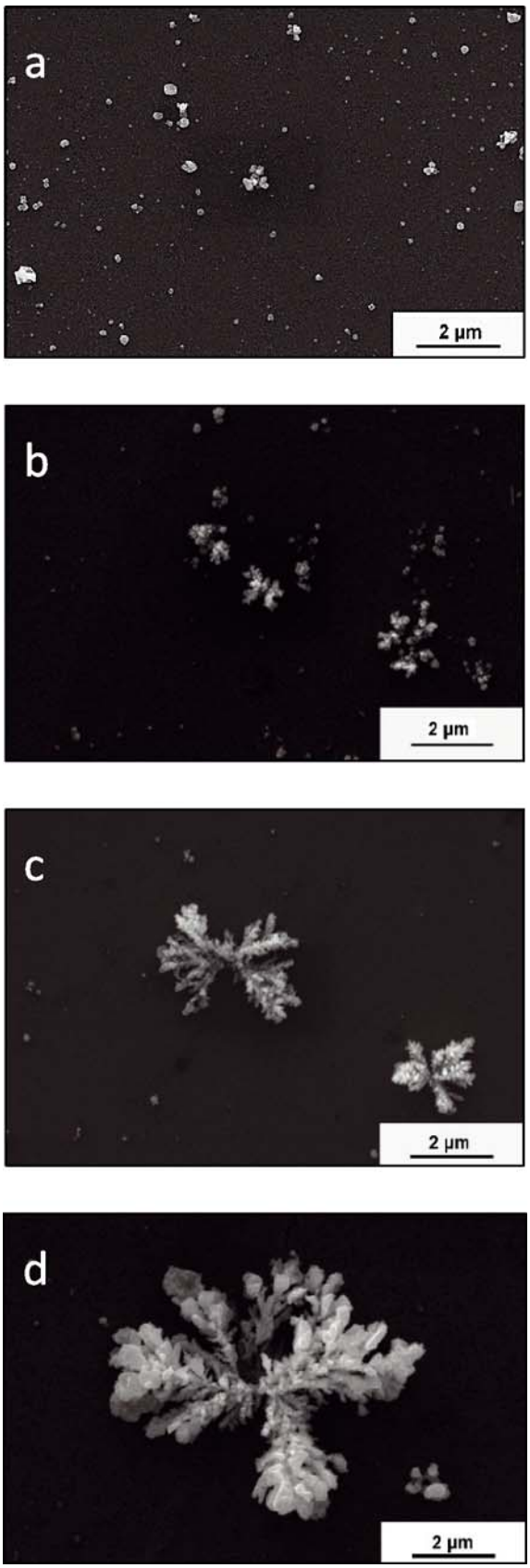

Figure 1. SEM micrographs of the Ag dendrites synthesized with deposition times of 1 min (a), 2.5 min (b), 5 min (c), and 20 min (d)

The structure of the electrodeposited Ag dendrites was examined using X-ray diffractometer. The XRD pattern is presented in Figure 3 which exhibited diffraction peaks at 2θ = 38.13, 53.67, 64.77, 76.32, and 81.52. These peaks correspond to the (111), (220), (331), and (222) planes, respectively. Compared to the pattern of JCPDS card number 00-004-0783, the measured pattern showed a very high

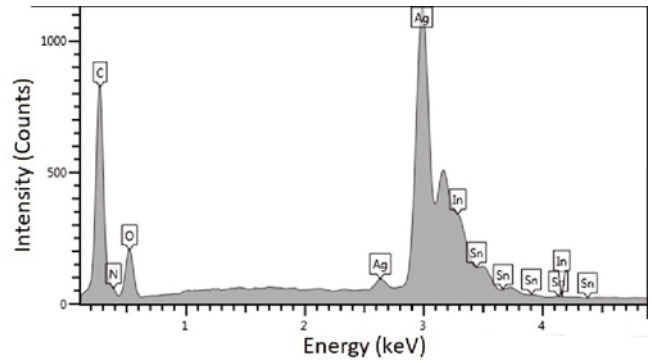

Figure 2. The EDX spectrum of the Ag dendrites electrodeposited for 20 minutes

intensity of (111) plane, while a peak of (200) was not observed. This could be attributed to the orientation growth of the deposit. To evaluate the preferred orientation of the structure, texture coefficient (TC) was determined from the XRD pattern by the following equation[28, 29].

$$TC_{(hkl)} = \frac{I_{(hkl)}/I_{o(hkl)}}{\frac{1}{N}\sum n I_{(hkl)}/I_{o(hkl)}} \quad (1)$$

where $I_{(hkl)}$ is the relative intensity of a plane experimentally measured for the specified plane, $Io_{(hkl)}$ is the standard intensity of the same plane taken from JCPDS card number 00-004-0783, N is the total number of reflections, and n is the number of diffraction peaks. The calculated values for the observed planes are shown in Table 1 that displays a high texture coefficient value of the (111) plane. Since a randomly texture presented by a texture coefficient of 1, this result indicates an abundance-oriented crystallite along the (111) plane. The high preferred orientation of the plane could be associated with the diffusion of the reduced Ag to a lower energy facet (111) that occurred during the pulse period of the lower potential (E_l) as discussed above.

Table 1. Texture coefficient of Ag dendrites

Plane	Texture Coefficient
111	1.98
220	0.81
311	0.3
222	0.9

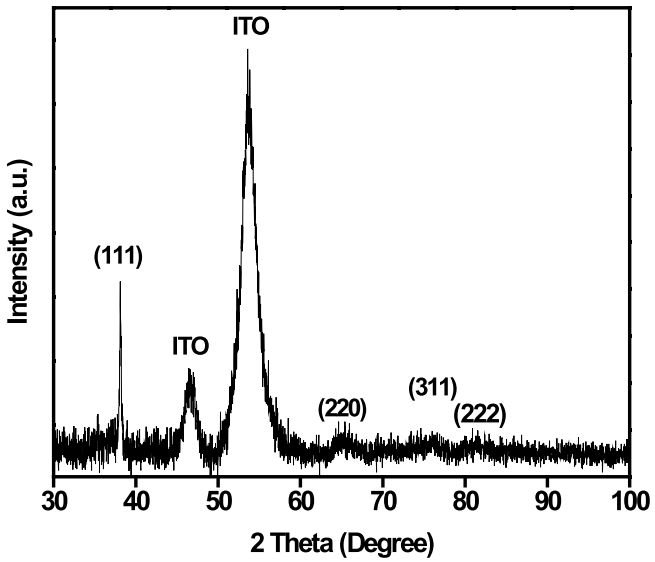

Figure 3. XRD pattern of Ag dendrites electrodeposited on the ITO substrate

Electrochemical analysis

Figure 4a shows Nyquist plots obtained from the EIS measurements. The plots indicate the intercept value at high frequencies and the equivalent series resistance (R_s) value, which include electrolyte resistance, inherent resistance, and contact resistance on the interface formed between electrolyte and the electrode surface[30]. It also shows the charge-transfer resistance (R_{ct}) or Faraday resistance correlated with the intercalation and deintercalation of the ions. Figure 4b presents the R_{ct} value of Ag deposits with different deposition times that shows a downward trend. The nanostructure of Ag dendrites exhibited the lowest charge transfer resistance (as low as 366.2 Ω) at a deposition time of 20 min. Lower R_{ct} values indicated good conductivity due to low internal electrode resistance, which could enhance the electrochemical activity of the material by reducing ion diffusion circuits[31]. Good electrical conductivity indicated faster charge transfer and larger capacitances, thus increasing the photocatalytic activity[32].

To further explore the electrochemical performance, the cell-specific capacitance of Ag dendrite deposits was evaluated from the cyclic voltammogram using the following equation[33].

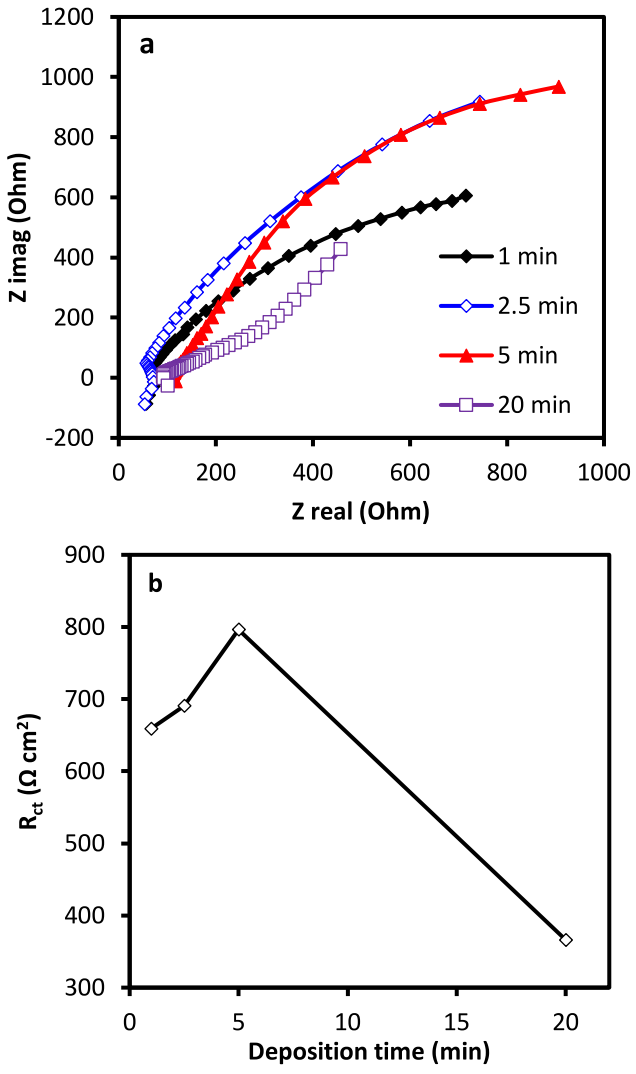

Figure 4. (a) Nyquist plots of Ag dendrites; (b) charge transfer resistance at different deposition times

$$C_s = \frac{\int I dV}{m \times SR \times V} \quad (2)$$

where I is current, m is active material mass, V is potential window, and SR is scan rate.

The comparison of the CV curves in terms of scan rates from 10 mV/s to 200 mV/s is shown in Figure 5a. The quasi-rectangular CV curve at a scan rate of 200 mV/s suggested that the electrode behaved as a pseudocapacitor. The calculated capacitances plot in Figure 5b shows that Ag dendrites at deposition time of 20 min delivered the highest specific capacitance (2.09 F/g). The specific value of larger capacitances was attributed to a larger specific surface area of the material[34]. Electrodes with larger surface areas showed enhanced photocatalytic activity due to their large number of active catalyst sites. Figure 5b exhibits a decrease in the specific capacitance value at higher scan rates. At low scan rates, the electrolyte might penetrate to the material more thoroughly and increase contact with the electrode surface, resulting in a high capacitance value[35]. Furthermore, at a high scan rate, the contact of ions in the electrolyte became finite, which then decreased the capacitance[36].

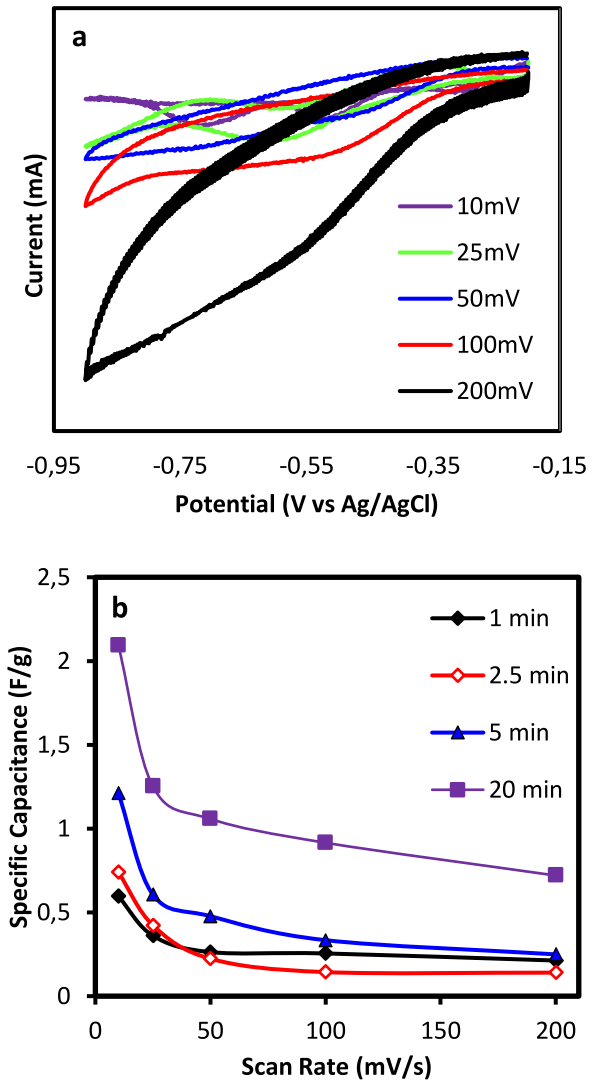

Figure 5. CV curves of the film deposited at different scan rates from 10 mV/s to 200 mV/s (a) and specific capacitance of the thin-film electrode versus scan rate (b)

Methylene Blue Photodegradation

The photocatalytic activity of Ag dendrites for methylene blue (MB) degradation was investigated under UV light irradiation. Figure 6 shows that the optical

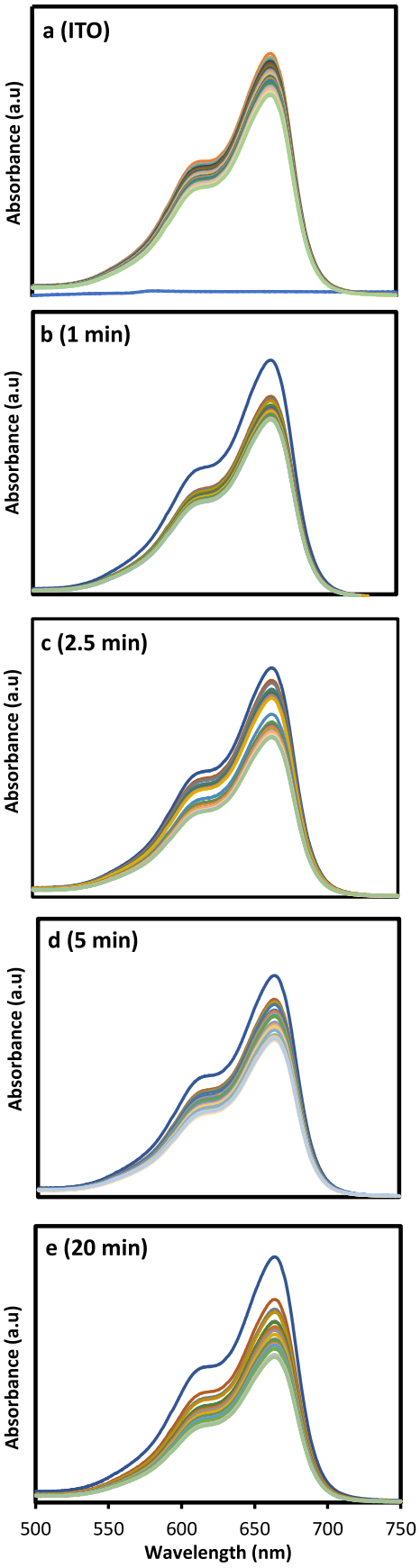

Figure 6. Absorbance spectra of methylene blue degradation using ITO (a) and Ag dendrites prepared with different deposition times (b–e)

absorbance of MB at the main absorption band (centering at 664 nm) rapidly decreased with time, indicating that it was degraded effectively. The percentage of MB degradation calculated using equation 3 is shown in Figure 7. The highest value was obtained at a deposition time of 20 min, and 45.57% of the MB had degraded after 30 min of UV irradiation.

$$\% \text{ degradation} = \frac{Co - Ct}{Co} \; x \; 100 \qquad (3)$$

where C_o = initial dye concentration and Ct = dye concentration after irradiation time t.

The mechanism underlying the photocatalytic degradation of MB can be understood as the role of active species, namely, superoxide radicals ($\bullet O^{2-}$) and hydroxyl radicals ($\bullet$OH), which act as strong oxidizing agents for MB. These species are formed when a water molecule is adsorbed onto silver dendrite active sites and dissociated due to the high energy surface, producing radicals[3, 4]. Therefore, the percentage of MB degradation increased when the deposition time of the catalyst increased. This should be attributed to the dendritic growth at longer deposition times (Fig. 1) which can increase the number of active sites to produce radicals. The wider dendritic structures also reduced the charge transfer resistance and increased the specific capacitance value which allowed the chemical reaction to take place at the catalyst-electrolyte interface.

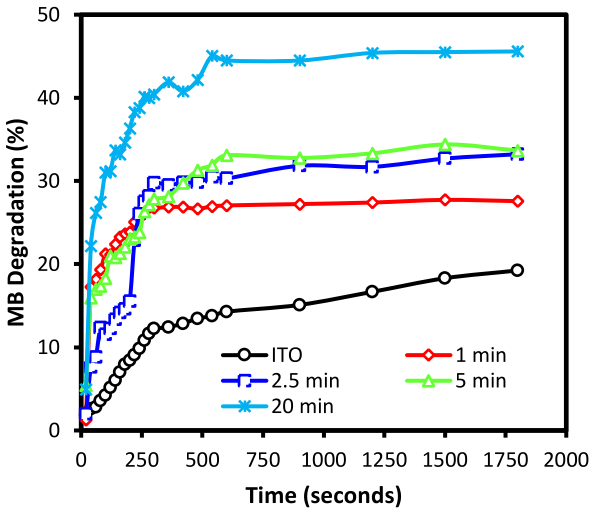

Figure 7. Photodegradation of methylene blue using Ag dendrite photocatalysis under UV radiation

CONCLUSION

Ag dendrite was synthesized from a surfactant-free electrolyte and the evolution of the morphology of dendritic structures was tuned by varying the deposition time. The potentials applied using the square wave voltammetry technique facilitate continuous nucleation and particle growth on the preferred (111) plane and thus produce a fractal structure of the Ag dendrites. The dendritic structure was found to grow continuously by increasing the deposition time. The expanded dendrites exhibit a plentiful active site that produced the smallest R_{ct} values due to a decrease in ion diffusion circuits, which indicated faster charge transfer and larger capacitances. The condition resulted in high photocatalytic activity for methylene blue degradation. This work has presented a simple route for the synthesis of Ag dendrites, which may have great potential for photocatalytic reactions.

ACKNOWLEDGMENTS

This work was supported by LPPM Universitas Negeri Jakarta under research scheme Penelitian Unggulan Universitas with contract number 33/KOMP-UNJ/LPPM/V/2020.

CONFLICTS OF INTEREST

The authors have declared no conflicts of interest regarding this published work.

LITERATURE CITED

1. Stoyanova, A., Bachvarova-Nedelcheva, A. & Iordanova R. (2018). Photocatalytic degradation of two azo-dyes in single and binary mixture by La modified Tio_2. *J. Chem. Technol. Metall*. 53(6), 1173–1178. DOI:

2. Opoku, F., Govender, K.K., Van Sittert, C.G.C.E. & Govender, PP. (2017). Recent Progress in the Development of Semiconductor-Based Photocatalyst Materials for Applications in Photocatalytic Water Splitting and Degradation of Pollutants. *Adv. Sustain Syst.* 1(7), 1–24. DOI:10.1002/adsu.201700006.

3. Umar, A.A., Rahmi, E., Balouch, A., Rahman, M.Y.A., Salleh, M.M. & Oyama, M. (2014). Highly-reactive AgPt nanofern composed of {001}-faceted nanopyramidal spikes for enhanced heterogeneous photocatalysis application. *J. Mater. Chem.* A 2(41), 17655–17665. DOI: DOI:10.1039/c4ta03518f.

4. Abdullah, N.A., Bakar, N.A., Shapter, J.G., Salleh, M.M. & Umar, A.A. (2017). Synthesis of silver-platinum nanoferns substrates used in surface-enhanced Raman spectroscopy sensors to detect creatinine. *Adv. Nat. Sci. Nanosci. Nanotechnol.* 8(2), 1–4. DOI:10.1088/2043-6254/aa687f.

5. Hammad, A., Anzai, A., Zhu, X., Yamamoto, A., Ootsuki, D., Yoshida, T., EL-Shazly, A., Elkady, M. & Yoshida, H. (2020). Photodeposition Conditions of Silver Cocatalyst on Titanium Oxide Photocatalyst Directing Product Selectivity in Photocatalytic Reduction of Carbon Dioxide with Water. *Catal Letters* 150(4), 1081–1088. DOI: 10.1007/s10562-019-02997-z.

6. Xie, J., Zeng, Y., Yang, X. & Xu, X. (2017). Electrodeposition of silver dendritic-graphene composite film for photocatalytic application. *Int. J. Electrochem. Sci.* 12(3), 1690–1699. DOI: 10.20964/2017.03.49.

7. Yin, X., Que, W. & Shen, F. (2011). ZnO nanorods arrays with Ag nanoparticles on the (002) plane derived by liquid epitaxy growth and electrodeposition process. Thin Solid Films 520(1), 186–192. DOI: 10.1016/j.tsf.2011.07.016.

8. Ding, C., Tian, C., Krupke, R. & Fang, J. (2012). Growth of non-branching Ag nanowires via ion migrational-transport controlled 3D electrodeposition. Cryst. Eng. Commun. 14(3), 875–879. DOI: 10.1039/c1ce05686g.

9. Li, Z., Du, Z. & He, X. (2017). Template-assisted electrodeposition of urchin-like Ag-nanoplate-assembled nanorod arrays and their structurally enhanced SERS performance. *J. Electrochem. Soc.* 164(13), 895–900. DOI: 10.1149/2.1351713jes.

10. Liu, S., Xu, Z., Sun, T., Zhao, W., Wu, X., Ma, Z., Zhang, X., He, J. & Chen, C. (2014). Polymer-Templated Electrodeposition of Ag Nanosheets Assemblies Array as Reproducible Surface-Enhanced Raman Scattering Substrate. *J. Nanosci. Nanotechnol.* 14(6), 4608–4614. DOI: 10.1166/jnn.2014.9036.

11. Fu, L., Wang, A., Zheng, Y., Cai, W. & Fu, Z. (2015). Electrodeposition of Ag dendrites/AgCl hybrid film as a novel photodetector. *Mater Lett* 142, 119–121. DOI: 10.1016/j.matlet.2014.12.001.

12. Dhanasmoro, L. & Budi, S. (2019). Surfactant-Free Electrodeposition of Ag Dendrites as Photocatalyst for Methylene

Blue Degradation. IOP Conf. Ser. Mater. Sci. Eng. 686(1), 1–6. DOI: 10.1088/1757-899X/686/1/012028.

13. Chan, Y.F., Zhang, C.X., Wu, Z.L., Zhao, D.M. & Wang, W. (2013). Ag dendritic nanostructures as ultrastable substrates for surface-enhanced Raman scattering Ag dendritic nanostructures as ultrastable substrates for surface-enhanced Raman scattering. *Appl. Phys. Lett*. 102, 1–5 DOI: 10.1063/1.4803937.

14. Hanafi, I., Daud, A.R., Radiman, S., Ghani, M.H.A. & Budi, S. (2013). Surfactant assisted electrodeposition of nanostructured CoNiCu alloys. *J. Phys. Conf. Ser.* 431(1), 1–6. DOI: 10.1088/1742-6596/431/1/012013.

15. Sivasubramanian, R. & Sangaranarayanan, M.V. (2015). A facile formation of silver dendrites on indium tin oxide surfaces using electrodeposition and amperometric sensing of hydrazine. *Sensors Actuators, B: Chem*. 213, 92–101. DOI: 10.1016/j.snb.2015.02.065.

16. Xia, L.T., Wei, G.Y., Li, M.G., Guo, H.F., Fu, Y. & Dettinger, H. (2014). Preparation of Co–Pt–P thin films by magnetic electrodeposition. *Mater. Res. Innov.* 18(5), 386–391. DOI: 10.1179/1433075X13Y.0000000154.

17. Zhou, Q., Wang, S., Jia, N., Liu, L., Yang, J. & Jiang, Z. (2006). Synthesis of highly crystalline silver dendrites microscale nanostructures by electrodeposition. *Mater. Lett*. 60(29–30), 3789–3792. DOI: 10.1016/j.matlet.2006.03.115.

18. Lee, J.K., Lee, J.S., Ahn, Y.S. & Kang, G.H. (2018). Effect of current density on morphology of silver thin film recovered from crystalline silicon solar cell by electrochemical process. Thin Solid Films 663, 143–147. DOI: 10.1016/j.tsf.2018.08.021.

19. Agrawal, V.V., Kulkarni, G.U. & Rao, C.N.R. (2008). Surfactant-promoted formation of fractal and dendritic nanostructures of gold and silver at the organic – aqueous interface. *J. Coll. Interface Sci.* 318(2), 501–506. DOI: 10.1016/j.jcis.2007.10.013.

20. Budi, S., Tawwabin, R.A., Cahyana, U. & Paristiowati, M. (2020). Saccharin-assisted Galvanostatic Electrodeposition of Nanocrystalline FeCo Films on a Flexible Substrate. *Int. J. Electrochem. Sci.* 15, 6682–6694. DOI: 10.20964/2020.07.74.

21. Budi, S., Kurniawan, B., Mott, D.M., Maenosono, S., Umar, A.A. & Manaf, A. (2017). Comparative trial of saccharin-added electrolyte for improving the structure of an electrodeposited magnetic FeCoNi thin film. Thin Solid Films 642, 51–57. DOI: 10.1016/j.tsf.2017.09.017.

22. Jiang, G., Wang, L.I., Chen, T.A.O., Yu, H. & Wang, J. (2005). Preparation and characterization of dendritic silver nanoparticles. *J. Mater. Sci.* 40, 1681–1683. DOI: 10.1007/s10853-005-0669-9.

23. Liu, J., Wang, X., Lin, Z., Cao, Y., Zheng, Z., Zeng, Z & Hu, Z. (2014). Electrochimica Acta Shape-Controllable Pulse Electrodeposition of Ultrafine Platinum Nanodendrites for Methanol Catalytic Combustion and the Investigation of their Local Electric Field Intensification by Electrostatic Force Microscope and Finite Element M. Electrochim Acta 136, 66–74. DOI: 10.1016/j.electacta.2014.05.082.

24. Inamuddin. (2019). Xanthan gum/titanium dioxide nanocomposite for photocatalytic degradation of methyl orange dye. *Int. J. Biol. Macromol.* 121, 1046–1053. DOI: 10.1016/j.ijbiomac.2018.10.064.

25. Yao, H., Li, F., Lutkenhaus, J., Kotaki, M. & Sue, H.J. (2016). High-performance photocatalyst based on nanosized ZnO-reduced graphene oxide hybrid for removal of Rhodamine B under visible light irradiation. *AIMS Mater. Sci*. 3(4), 1410–1425. DOI: 10.3934/matersci.2016.4.1410.

26. Cheng, Z.Q., Li, Z.L., Luo, X., Shi, H.Q., Luo, C.L., Liu, Z.M. & Nan, F. (2019). Enhanced second harmonic generation by double plasmon resonances in mesoscale flower-like silver particles. *Appl. Phys. Lett.* 114(1), 1–4. DOI: 10.1063/1.5079241.

27. Bu, Y. & Lee, S.W. (2015). Flower-like gold nanostructures electrodeposited on indium tin oxide (ITO) glass as a SERS-active substrate for sensing dopamine. *Microchim. Acta* 182(7–8), 1313–1321. DOI: 10.1007/s00604-015-1453-4.

28. Caglar, M. Ilican, S. Caglar, Y. & Yakuphanoglu, F. (2009). Electrical conductivity and optical properties of ZnO nanostructured thin film. *Appl. Surf. Sci.* 255(8), 4491–4496. DOI: https://doi.org/10.1016/j.apsusc.2008.11.055.

29. Huang, J.H. Lin, C.H. & Yu, G.P. (2019). Texture evolution of vanadium nitride thin films. Thin Solid Films 688, 137-415. DOI: 10.1016/j.tsf.2019.137415.

30. Rakhi, R.B., Chen, W., Cha, D. & Alshareef, H.N. (2012). Substrate Dependent Self-Organization of Mesoporous Cobalt Oxide Nanowires with Remarkable Pseudocapacitance. Nano Lett 12, 2559–2567. DOI:

31. Yin, B., Zhang, S., Jiao, Y., Liu, Y., Qu, F. & Wu, X. (2014). Facile synthesis of ultralong MnO2 nanowires as high performance supercapacitor electrodes and photocatalysts with enhanced photocatalytic activities. *Cryst. Eng.* 16(43), 9999–10005. DOI: 10.1039/c4ce01302f.

32. Beura, R., Pachaiappan, R. & Thangadurai P. (2018). A detailed study on Sn4+doped ZnO for enhanced photocatalytic degradation. Appl. Surf. Sci. 433, 887–898. DOI: 10.1016/j.apsusc.2017.10.127.

33. Oraon, R., De Adhikari, A., Tiwari, S.K. & Nayak, G.C. (2016). Enhanced Specific Capacitance of Self-Assembled Three-Dimensional Carbon Nanotube/Layered Silicate/Polyaniline Hybrid Sandwiched Nanocomposite for Supercapacitor Applications. *ACS Sustain Chem. Eng.* 4(3), 1392–1403. DOI: 10.1021/acssuschemeng.5b01389.

34. Daraghmeh, A., Hussain, S., Saadeddin, I., Servera, L., Xuriguera, E., Cornet, A. & Cirera, A. (2017). A Study of Carbon Nanofibers and Active Carbon as Symmetric Supercapacitor in Aqueous Electrolyte: A Comparative Study. *Nanoscale Res. Lett.* 12(639), 1–10. DOI: 10.1186/s11671-017-2415-z.

35. Mishra, N., Shinde, S., Vishwakarma, R., Kadam, S., Sharon, M. & Sharon, M. (2013). MWCNTs synthesized from waste polypropylene plastics and its application in super-capacitors. AIP Conf. Proc. 1538, 228–236. DOI: 10.1063/1.4810063.

36. Arul, N.S., Mangalaraj, D., Ramachandran, R., Grace, A.N. & Han, J.I. (2015). Fabrication of CeO2/Fe2O3 composite nanospindles for enhanced visible light driven photocatalysts and supercapacitor electrodes. *J. Mater. Chem*. A: 3(29), 15248–15258. DOI: 10.1039/c5ta02630j.